Coulomb blockade and Kondo effect in the electronic structure of Hubbard molecules connected to metallic leads: A finite-temperature exact-diagonalization study

H. Ishida[1,2] and A. Liebsch[2]

[1]*College of Humanities and Sciences, Nihon University, Tokyo 156-8550, Japan*
[2]*Peter Grünberg Institute and Institute of Advanced Simulations, Forschungszentrum Jülich, 52425 Jülich, Germany*

The electronic structure of small Hubbard molecules coupled between two noninteracting semi-infinite leads is studied in the low bias-voltage limit. To calculate the finite-temperature Green's function of the system, each lead is simulated by a small cluster, so that the problem is reduced to that of a finite-size system comprising the molecule and clusters on both sides. The Hamiltonian parameters of the lead clusters are chosen such that their embedding potentials coincide with those of the semi-infinite leads on Matsubara frequencies. Exact diagonalization is used to evaluate the effect of Coulomb correlations on the electronic properties of the molecule at finite temperature. Depending on key Hamiltonian parameters, such as Coulomb repulsion, one-electron hopping within the molecule, and hybridization between molecule and leads, the molecular self-energy is shown to exhibit Fermi-liquid behavior or deviations associated with finite low-energy scattering rates. The method is shown to be sufficiently accurate to describe the formation of Kondo resonances inside the correlation-induced pseudogaps, except in the limit of extremely low temperatures. These results demonstrate how the system can be tuned between the Coulomb blockade and Kondo regimes.

I. INTRODUCTION

Finite-size electron systems linked to noninteracting electron reservoirs have been a topic of intense theoretical and experimental study because of their relevance to quantum dot systems and single-molecule devices. Depending on the importance of correlation effects induced by the electron-electron Coulomb repulsion, different types of theoretical approaches are employed. For weakly correlated systems, ballistic electron transport is studied within the one-electron approximation such as density-functional theory (DFT).[1–5] On the other hand, strongly correlated systems are modeled by tight-binding Hamiltonians with Hubbard- or Anderson-type interaction terms and various many-body techniques are applied.[6–33] Two noticeable effects beyond the one-electron approximation are the Kondo effect and Coulomb blockade, both of which are observed in quantum dot systems.[34–36] More recently, the Kondo effect was also observed in adsorbed molecules by scanning tunneling spectroscopy and high-resolution photoemission spectroscopy.[37–40] The Kondo effect in nanosize systems was studied theoretically by using the numerical renormalization group (NRG) technique for a variety of cases, such as multidot or multilevel systems and dots coupled to superconducting leads,[16–21] within DFT combined with the one-crossing approximation[23–26] and the continuous-time quantum Monte Carlo technique.[27] Coulomb blockade effects seen in electron transport through a finite-size interacting system are investigated by using rate-equation techniques and nonequilibrium Green's function theory.[29–33]

The aim of the present work is to introduce a scheme for the investigation of quantum dots that is applicable in the full range between Kondo physics and Coulomb blockade, except in the limit of extremely low Kondo temperatures. To illustrate this approach, we focus on small interacting molecules coupled to noninteracting semi-infinite electron reservoirs. The many-body properties of these systems are evaluated by using exact diagonalization (ED) at finite temperatures.[41–43] In order to apply ED, the semi-infinite leads are simulated by finite-size clusters. For a given chemical potential, the tight-binding Hamiltonian parameters of these clusters are chosen such that the difference between the surface-site Green's function of a semi-infinite lead and the corresponding cluster lead is minimized along the Matsubara axis. The finite-temperature Green's function of the total system consisting of molecule and lead clusters is then evaluated exactly within ED. Since the effective lead-cluster Hamiltonian is extremely sparse, at typical temperatures of interest only a limited number of excited states needs to be evaluated. Here we consider Hubbard chain and ring molecules attached to two metallic leads. In these systems lead clusters consisting of only five bath levels can accurately mimic the true embedding potentials down to $T \gtrsim t_M/500$, where t_M denotes the hopping parameter representing the metallic leads. Thus, the formation of Kondo resonances within the correlation-induced pseudogaps can be investigated. In the case of a single Hubbard atom coupled to a single lead, the problem reduces to the single-impurity Anderson model. The cluster size can then be significantly increased so that much lower temperatures can be reached. An additional advantage of our method is that the zero-bias-voltage limit of the interacting system can be studied for arbitrary values of the Coulomb repulsion and molecule-lead hybridization, without further approximations.

The discretization of the semi-infinite leads and the application of ED to the resulting finite-size system is analogous to the use of ED as impurity solver within the context of dynamical mean-field theory (DMFT) and its cluster extensions,[44–46] where the Weiss mean field is represented by a finite number of noninteracting levels. Multiorbital as well as multisite correlations have been studied for a variety of materials,[43] including various surfaces and heterostructures.[47] The main difference is that in the present case the leads are assumed to be noninteracting, so that the self-consistent iterative procedure is absent.

An important feature of the ED approach is that it provides complete dynamical information, in particular, transfer of spectral weight between low and high excitation energies, formation of Hubbard bands, and opening of correlation-induced pseudogaps. A quantity of central interest therefore is the molecular self-energy which exhibits strong variations as a function of Hamiltonian parameters and temperature. In particular, Fermi-liquid behavior in the Kondo regime and correlation-induced finite scattering rates in the Coulomb blockade regime can clearly be identified.

The outline of this paper is as follows. In Sec. II we describe our theoretical model for the molecule-lead system and discuss several details of the calculation of the molecular self-energy and interacting Green's function. In Sec. III we present the numerical results and the discussion, with special emphasis on the Coulomb blockade and Kondo effect. Section IV contains the summary. In the Appendix we consider a single adatom on a semi-infinite lead and examine the temperature range in which a finite-size cluster can be used to simulate a semi-infinite lead. Since this case is equivalent to the single-impurity Anderson model, the results can directly be compared with those of other schemes that are applicable at arbitrarily low temperatures.

II. THEORY

A. Formalism

We consider a molecule consisting of N atomic sites and linked to two semi-infinite metal leads, as shown schematically in Fig. 1(a). The isolated molecule is modeled by a multisite Hubbard Hamiltonian characterized by the onsite energy ϵ_a,
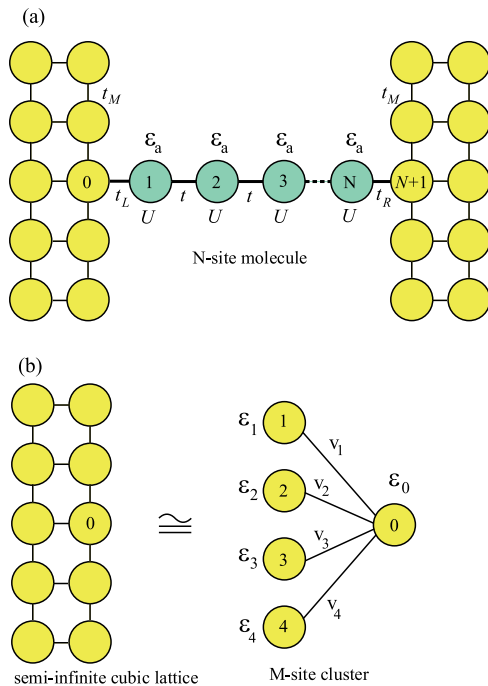

(a)

(b)

semi-infinite cubic lattice   M-site cluster

FIG. 1. (Color online) (a) Tight-binding model for an N-site molecule attached to two noninteracting semi-infinite leads. (b) For the evaluation of the Green's function of the molecule, the two semi-infinite leads are replaced by a cluster consisting of M levels, as shown here schematically for the left lead.

the nearest-neighbor hopping interaction t, and the onsite Coulomb repulsion U,

$$\hat{h}_C = \sum_{i\sigma} \epsilon_a \hat{n}_{i\sigma} - \sum_{\langle i,j\rangle\sigma} t\, \hat{c}^\dagger_{i\sigma}\hat{c}_{j\sigma}, + \sum_i U\, \hat{n}_{i\uparrow}\hat{n}_{i\downarrow}, \quad (1)$$

where $\hat{c}^\dagger_{i\sigma}$ ($\hat{c}_{i\sigma}$) creates (destroys) an electron with spin σ at site i ($1 \leqslant i \leqslant N$), $\hat{n}_{i\sigma} = \hat{c}^\dagger_{i\sigma}\hat{c}_{i\sigma}$, and the summation in the second term is taken over pairs of nearest neighbors. Hereafter, we adopt the notation where the matrix (operator) corresponding to a quantity A is denoted by $\hat{A}$ while its matrix elements are defined as A_{ij}. For simplicity, we limit the discussion here to one level per molecular site and purely onsite Coulomb interactions. Equivalently, it would also be feasible to investigate multiorbital interactions, including interorbital Coulomb and Hund's rule coupling, for instance, in transition metal ions attached to semi-infinite leads. Throughout this paper, the hopping integral within the molecule is taken as unit of the energy scale, that is, $t = 1$.

The left (right) lead is represented by noninteracting electrons on a semi-infinite simple cubic lattice with nearest-neighbor hopping interaction t_M and the onsite energy level is chosen as zero of the energy scale:

$$\hat{h}_{L(R)} = -\sum_{\langle i,j\rangle\sigma} t_M\, \hat{c}^\dagger_{i\sigma}\hat{c}_{j\sigma}, \quad (2)$$

where $i,j < 1$ ($i,j > N$), so that the energy bands of both leads exhibit a finite density of states (DOS) in the energy range $[-6t_M, 6t_M]$.

The molecule is linked to the left (right) lead via the hopping integral between site 1 (N) of the molecule and site 0 ($N+1$) of the left (right) lead. The mixing term of the Hamiltonian describing the molecule-lead hybridization is expressed as

$$\hat{h}_{\text{mix}} = -\sum_\sigma (t_L \hat{c}^\dagger_{0\sigma}\hat{c}_{1\sigma} + t_R \hat{c}^\dagger_{N+1\sigma}\hat{c}_{N\sigma}) + \text{H.c.}, \quad (3)$$

where, for simplicity, the hopping integrals on both sides are assumed to coincide: $t_L = t_R$. The Hamiltonian of the total system consisting of the molecule and the two leads is given by

$$\hat{H} = \hat{h}_C + \hat{h}_L + \hat{h}_R + \hat{h}_{\text{mix}}. \quad (4)$$

We investigate the electronic structure of the molecule described by Eq. (4) for a wide range of Hamiltonian parameters. As we consider the low bias-voltage limit, both leads have the same chemical potential, which is denoted as μ. The Green's function $\hat{G}$ of the molecule can be written as

$$G_{ij}(i\omega_n) = \big[i\omega_n + \mu - \hat{h}_C^0 - \hat{\Sigma}(i\omega_n) \\ - \hat{s}^L(i\omega_n + \mu) - \hat{s}^R(i\omega_n + \mu)\big]^{-1}_{ij}, \quad (5)$$

where $1 \leqslant i,j \leqslant N$, $\omega_n = (2n+1)\pi T$ ($n \geqslant 0$) are Matsubara frequencies at temperature T, $\hat{h}_C^0$ denotes the first two terms of Eq. (1), and $\hat{\Sigma}(i\omega_n)$ is the self-energy matrix accounting for electron correlation effects within the molecule. As we also allow for interatomic Coulomb correlations, the self-energy matrix has off-diagonal components with respect to site index. This approach differs from recent ones[23–26] in which the self-energy of each site is assumed to be local and determined in a self-consistent manner similarly to the layer

DMFT approach.[48] In the present work, we consider only paramagnetic solutions and omit the spin index σ hereafter. In Eq. (5), $\hat{s}^{L(R)}$ denotes the embedding potential describing the one-electron hybridization effects due to the left (right) lead on the molecule.[49,50] These embedding potentials give rise to broadening and shifting of the molecular levels and therefore play the role of contact self-energies.[13]

For the present geometry, only the $\{11\}$ element of $\hat{s}^L$ is nonvanishing:

$$s_{11}^L(z) = t_L^2 [z - \hat{h}_L]_{00}^{-1} = t_L^2\, g_{00}(z). \qquad (6)$$

Similarly, the only nonvanishing element of $\hat{s}^R$ is

$$s_{NN}^R(z) = t_R^2 [z - \hat{h}_R]_{N+1,N+1}^{-1} = t_R^2\, g_{N+1,N+1}(z). \qquad (7)$$

The surface Green's functions appearing in these expressions are given by

$$g_{ii}(z) = \int_{-6t_M}^{6t_M} d\epsilon\, \frac{\rho_i(\epsilon)}{z - \epsilon}, \qquad (8)$$

where $\rho_i(\epsilon)$ denotes the local density of states per spin at surface site i within the left ($i = 0$) or right ($i = N + 1$) lead.

In order to make use of ED for the evaluation of the interacting Green's function of the molecule [Eq. (5)], we follow a procedure that has proved to be very useful in analogous DMFT calculations. The surface Green's functions $g_{ii}(z)\,(i = 0, N + 1)$ representing the continuous spectra of the leads are approximated by those of finite clusters consisting of M levels, as depicted in Fig. 1(b) for the left lead. The $\{00\}$ element of the cluster Green's function is given by

$$g_{00}^{cl}(z) = \left[z - \epsilon_0 - \sum_{k=1}^{M-1} \frac{v_k^2}{z - \epsilon_k} \right]^{-1}, \qquad (9)$$

where ϵ_k ($0 \leqslant k \leqslant M - 1$) and v_k ($1 \leqslant k \leqslant M - 1$) are the energy levels and intracluster hybridizations, respectively. An analogous expression holds for the surface Green's function of the right lead, $g_{N+1,N+1}(z)$. (Note that the cluster levels ϵ_k do not refer to actual lattice sites within the leads. Instead, they represent auxiliary quantities to simulate the spectral distributions of the leads.) The discretization of $g_{00}(z)$ is not suitable on the real energy axis since $g_{00}(z)$ has a continuous energy spectrum while $g_{00}^{cl}(z)$ possesses only a finite number of poles. Thus, $\mathrm{Im}\, g_{00}^{cl}(z) \to 0$ or $-\infty$ in the limit $z \to 0$, whereas $g_{00}(z)$ for metallic leads remains finite, so that, in the very low-energy region, the cluster Green's function deviates strongly from the actual lead Green's function. These discrepancies are absent if the calculation is restricted to finite temperatures. $g_{00}(z)$ can then accurately be fitted by $g_{00}^{cl}(z)$ at Matsubara frequencies, since both functions vary smoothly along the imaginary energy axis. As shown in Ref. 43, in finite-T ED/DMFT calculations for typical multi-orbital materials, two or three bath levels per orbital are adequate to achieve adequate fits for temperatures in the range $T \approx W/50, \ldots, W/200$, where W is the bandwidth. For the present case, this implies $T \approx 0.025, \ldots, 0.10$. To reach lower temperatures therefore requires accordingly larger lead clusters.

As in standard ED/DMFT calculations, for a given chemical potential μ, the discretization of $g_{00}(z)$ can be achieved by determining ϵ_k and v_k in Eq. (9) via minimization of the quantity[43]

$$I = \sum_n W_n \mid g_{00}(i\omega_n + \mu) - g_{00}^{cl}(i\omega_n + \mu) \mid^2, \qquad (10)$$

where the weight function W_n is chosen as $1/\omega_n$ in order to provide greater accuracy at low ω_n. [The large frequency behavior is less relevant in this fit since both Green's functions approach $1/(i\omega_n)$ at large ω_n.] Other choices, such as $W_n = 1$ or $W_n = 1/\omega_n^2$, usually give very similar results, even though the auxiliary cluster parameters ϵ_k and v_k may vary slightly. With decreasing temperature T the lowest Matsubara frequency approaches the real energy axis, so that the fitting becomes less accurate. As is demonstrated in the next section and the Appendix, the true lead Green's function can be simulated by that of a relatively small five-level cluster with sufficient accuracy as long as the temperature is approximately in the range $T \gtrsim t_M/800$. Moreover, the lower boundary of this temperature range can be reduced by increasing the cluster size. As a consequence, it is feasible to describe the Kondo effect on the spectral density if the associated Kondo temperature is comparable with this temperature range.

It should be noted here that the Matsubara temperature used in the fitting of the lead surface Green's function may be viewed as a fictitious temperature T_M that does not need to coincide with the physical temperature T. Instead, its choice is mainly determined by the number of cluster levels used to simulate the semi-infinite leads. Evidently, a larger value of M permits fitting at lower values of T_M. This point is addressed further in the Appendix, where an extremely small value of T_M is chosen for the evaluation of the self-energy of a single adatom over a wide range of real temperatures. In most applications discussed below the Matsubara temperature is taken to be the physical temperature.

Let us denote the noninteracting Green's function of the molecule linked to the two semi-infinite leads by $\hat{G}^0$ and that linked to the two clusters by $\hat{G}^{0,cl}$, where the term "noninteracting" signifies $U = 0$ in the molecule. The interacting counterparts are $\hat{G}$ and $\hat{G}^{cl}$, respectively. When the tight-binding parameters of the lead clusters are optimized as described above, one can presume that $\hat{G}^0(i\omega_n) \approx \hat{G}^{0,cl}(i\omega_n)$ at all Matsubara frequencies. As a result, when the Coulomb interaction in the molecule is switched on, $\hat{G}(i\omega_n)$ should nearly coincide with $\hat{G}^{cl}(i\omega_n)$. We may therefore employ $\hat{G}^{cl}$ as a reasonable representation of the true interacting Green's function, $\hat{G}$, of the molecule attached to the two semi-infinite leads. Schematically, the procedure outlined above proceeds via the following steps:

$$\hat{g} \approx \hat{g}^{cl} \to \hat{G}^{cl} \approx \hat{G}. \qquad (11)$$

Below we do not distinguish between the molecular Green's functions $\hat{G}$ and $\hat{G}^{cl}$. We emphasize, however, that even if $\hat{G}$ agrees well with $\hat{G}^{cl}$ at Matsubara points, at real energies $\hat{G}^{cl}$ has a discrete level spectrum while that of $\hat{G}$ is continuous.

The Hamiltonian of the interacting molecule linked to the two M-level clusters is highly sparse. To compute $\hat{G}^{cl}(i\omega_n)$, we therefore make use of the Arnoldi algorithm, which is ideally suited to evaluate the lowest eigenstates relevant at temperature T. $\hat{G}^{cl}(i\omega_n)$ is then derived via the Lanczos procedure for a finite number of excited states. In the present work, system sizes up to $n_s = N + 2M = 15$ have been investigated. More

details concerning the numerical procedure are provided in Refs. 42 and 43. (As mentioned earlier, the approach outlined above does not involve any self-consistency procedure as in DMFT since the leads are uncorrelated. Their fixed electronic structure merely governs the boundary conditions of the interacting molecule. The auxiliary lead quantities ϵ_k and v_k characterizing the leads are therefore determined before carrying out the ED.)

B. Semi-infinite vs cluster leads

As discussed above, the calculation of the electronic structure of an interacting molecule between semi-infinite leads is made feasible by simulating the {00} ({$N+1, N+1$}) surface element of the Green's function of the left (right) lead in terms of a cluster Green's function, as indicated in Eq. (9). To demonstrate the accuracy of this fitting procedure, we compare in Fig. 2 both quantities as a function of ω_n for three values of μ for a semi-infinite lead with $t_M = 1$ (bandwidth $W = 12$).

The lead clusters consist of five levels. Thus, for $\mu \neq 0$, there are in total nine independent fit parameters: ϵ_k ($0 \leqslant k \leqslant 4$) and v_k ($1 \leqslant k \leqslant 4$). At half-filling ($\mu = 0$), this number is
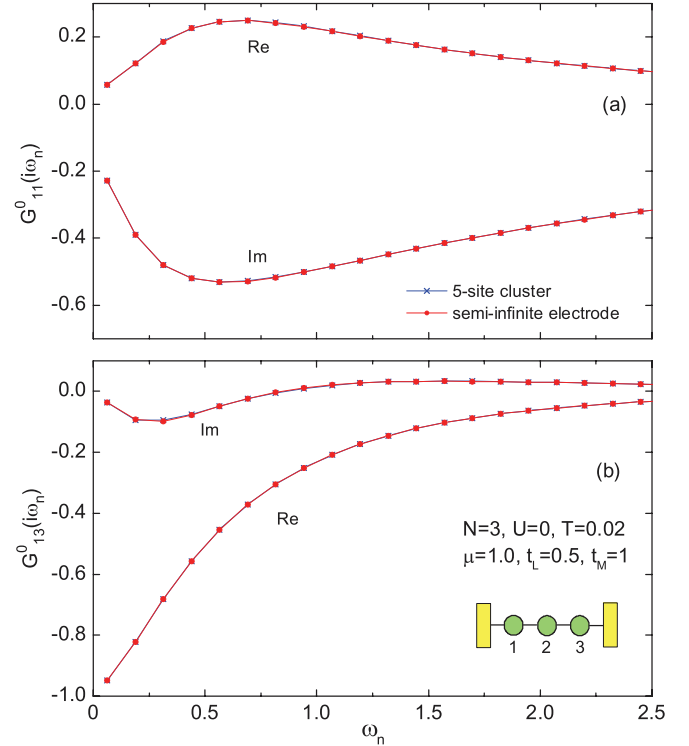
FIG. 3. (Color online) Noninteracting Green's function of a linear molecule with $N = 3$ between two semi-infinite leads (solid circles) and that between two five-level clusters (crosses). (a) Diagonal {11} element and (b) off-diagonal {13} element, for $t_M = 1$, $t_L = 0.5$, $\mu = 1.0$, and $T = 0.02$.

reduced to four because of symmetry reasons: $\epsilon_0 = 0$ and the other four levels are symmetrically distributed with respect to $\epsilon = 0$. The fitting then becomes slightly less accurate than away from half-filling. For the present choice of $T = 0.02$, $g_{00}(i\omega_n)$ is seen to agree very well with $g_{00}^{cl}(i\omega_n)$ in the whole ω_n range. At small Matsubara frequencies weak cusps appear in the cluster Green's function as a result of its singular behavior along the real energy axis.

Figure 2 suggests that the embedding potentials of the semi-infinite leads in Eq. (5) can be approximated at Matsubara points by those of small clusters. To illustrate this point further, we compare in Fig. 3 the resultant noninteracting Green's function of a linear molecule ($N = 3$) between two semi-infinite leads, $G_{ij}^0(i\omega_n)$, with the one of the same molecule between two five-level clusters, $G_{ij}^{0,cl}(i\omega_n)$. The Hamiltonian parameters correspond to those in Fig. 2(b) and the contact integrals are chosen as $t_L = 0.5$. It is seen that both the diagonal and off-diagonal elements of $G_{ij}^0(i\omega_n)$ are in excellent agreement with the corresponding cluster elements $G_{ij}^{0,cl}(i\omega_n)$.

A crucial question determining the usefulness of the approach outlined above concerns the range of temperatures in which accurate results can be obtained for a given cluster size. To explore this point, we present in the Appendix a careful study of the electronic structure of a single correlated adatom on a semi-infinite lead. In this case, a large range of cluster sizes can be employed in order to systematically investigate the behavior of the self-energy at very low temperatures. Cluster sizes up to $M = 11$ were used for $T \gtrsim t_M/1600$. The results

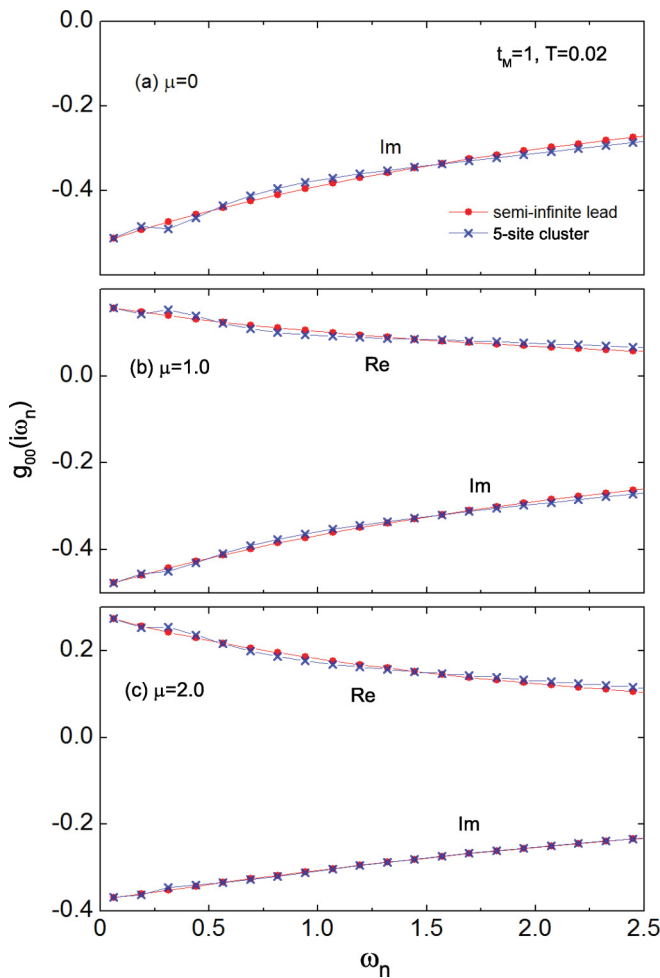FIG. 2. (Color online) Comparison of the {00} element of the Green's function of a semi-infinite lead (solid circles) and that of a five-level cluster (crosses). (a) $\mu = 0$, (b) $\mu = 1$, and (c) $\mu = 2$ for $t_M = 1$ and $T = 0.02$. The real part of g_{00} vanishes for $\mu = 0$.

for five-site clusters are found to agree quantitatively with those of larger clusters for $T \gtrsim t_M/500$ and qualitatively for $T \gtrsim t_M/800$. These results, together with the ones shown in Figs. 2 and 3, demonstrate the usefulness of our strategy of evaluating the Green's function of the Hubbard molecule by simulating the semi-infinite metallic leads in terms of finite clusters. In the following, we present results for the electronic structure of various linear and ring molecules, where the true leads are replaced by clusters consisting of five levels.

C. Spectral information

To demonstrate how the molecular electronic structure undergoes a transition between the Kondo and Coulomb blockade regimes, we consider in the next section the partially integrated local one-electron density of states which is defined as

$$\bar{\rho}_i(\mu) = -G_{ii}(\tau = \beta/2), \quad (12)$$

where $G_{ii}(\tau)$ is the diagonal component of the imaginary-time Green's function at site i ($\beta = 1/T$),

$$G_{ii}(\tau) = -\int d\omega \tilde{\rho}_i(\omega) \frac{e^{-\omega\tau}}{1 + e^{-\omega\beta}}$$
$$= T \sum_n e^{-i\omega_n\tau} G_{ii}(i\omega_n), \quad (13)$$

and the interacting local one-electron DOS is defined by

$$\tilde{\rho}_i(\omega) = -\frac{1}{\pi} \text{Im} G_{ii}(\omega + i\delta), \quad (14)$$

with a positive infinitesimal δ. $\bar{\rho}_i(\mu)$ may therefore be expressed as

$$\bar{\rho}_i(\mu) = -T \sum_n e^{-i\omega_n\beta/2} G_{ii}(i\omega_n)$$
$$= \int_{-\infty}^{\infty} d\omega \, F(\omega) \, \tilde{\rho}_i(\omega), \quad (15)$$

where $F(\omega) = 0.5/\cosh(\beta\omega/2) = (-T\partial f/\partial\omega)^{1/2}$ is a distribution of half-width $w = 4\ln(2 + \sqrt{3})T = 5.268T$ centered about $\omega = 0$ (f is the Fermi function). Thus, at a given value of the chemical potential μ, $\bar{\rho}_i(\mu)$ represents the local one-electron DOS of site i partially integrated within a few T around μ. The advantage of studying this quantity, as compared to the actual interacting DOS $\tilde{\rho}_i(\omega)$, is that it can be evaluated without extrapolating the Green's function from Matsubara frequencies toward the real energy axis.

We also note that the weight function $F(\omega)$ in $\bar{\rho}_i(\mu) = -G_{ii}(\beta/2)$ is closely related to the one appearing in the conductance of single atoms attached to leads. In this case the weight function is given by[51] $F_c(\omega) = -\partial f/\partial\omega$ with half-width $w_c = 2\ln(3 + \sqrt{2})T = 3.525T$. Thus, $\bar{\rho}_i(\mu)$ samples the molecular density of states near μ in a window ~ 1.5 times larger than in the case of the conductance.

We point out here that one can, of course, also evaluate the molecular Green's function G_{ij}^{cl} close to the real-energy axis. However, these spectra consist of many sharp peaks related to the finite number of levels of the lead clusters. Moreover, the level energies ϵ_k and intracluster coupling terms v_k depend not only on the cluster size, but also on the choice of the weight

function W_n in Eq. (10). Evidently, one would have to use very large lead clusters so that these discrete spectra evolve into a meaningful representation of the continuous spectra of the actual semi-infinite leads. Because of the exponentially growing Hilbert space the ED approach would then no longer be practical. Thus, the purpose of introducing the auxiliary fit parameters ϵ_k and v_k is to simulate the finite-temperature lead Green's functions and embedding potentials at Matsubara points. At not too low T, these functions converge very well with cluster size and are remarkably stable against variations in ϵ_k and v_k and for different choices of W_n.[43] The continuous spectra of the Green's function elements $G_{ij}(\omega)$ describing the molecule attached to semi-infinite leads may then be derived via analytic continuation of $G_{ij}(i\omega_n)$ or, preferably, of the molecular self-energy $\Sigma_{ij}(i\omega_n)$ to real energies. In the latter case, continuation of the known one-electron properties of the molecule and of the leads is avoided. The task of analytically continuing $G_{ij}(i\omega_n)$ or $\Sigma_{ij}(i\omega_n)$ is entirely analogous to the one in quantum Monte Carlo simulations, where the maximum entropy scheme is often used to generate real energy spectra. In DMFT studies the discrete Green's functions $G_{ij}^{cl}(\omega)$ can, however, be very useful for the identification of a Mott transition since the excitation gap opens at the same critical Coulomb interaction as in the continuous spectrum of $G_{ij}(\omega)$.

III. RESULTS AND DISCUSSION

A. Noninteracting molecules

To provide an impression of the electronic structure of the molecule in the absence of Coulomb interactions, we show first in Fig. 4 $\rho_{av}(\epsilon)$, the noninteracting local DOS averaged over all sites, for linear and ring molecules with $N = 4$ linked between two semi-infinite leads, where $t_M = 1$ and $t_L = 0.5$. In the following, the onsite energy ϵ_a is specified as $-U/2$, so that the system becomes electron-hole symmetric when it is half-filled. For linear molecules, the DOS consists of N resonant peaks corresponding to the energy levels e_m of the isolated molecule, which are distributed symmetrically with respect to $\epsilon = 0$. The lowest energy state has even parity with respect to the center of gravity of the molecule, and the parity alternates in the order of ascending energy levels. The energy width of the mth resonance, which is determined by its coupling to the imaginary part of the lead embedding potentials, is given by

$$\Gamma_m = \pi t_L^2 [\rho_0(e_m)|\psi_m(1)|^2 + \rho_{N+1}(e_m)|\psi_m(N)|^2], \quad (16)$$

where $\psi_m(i)$ denotes the amplitude at site i of the electron wave function of the mth level of the isolated molecule with energy e_m. It is understood that the lowest level corresponds to index $m = 1$. For the ring molecule in Fig. 4(b), the DOS exhibits only three peaks, since the central one at $\epsilon = 0$ is doubly degenerate. The wave functions of the isolated ring molecule in the site basis are

$$|\psi_1\rangle = \frac{1}{2}(|1\rangle + |2\rangle + |3\rangle + |4\rangle), \quad |\psi_2\rangle = \frac{1}{\sqrt{2}}(|2\rangle - |3\rangle),$$

$$|\psi_3\rangle = \frac{1}{\sqrt{2}}(|1\rangle - |4\rangle), \quad |\psi_4\rangle = \frac{1}{2}(|1\rangle - |2\rangle - |3\rangle + |4\rangle).$$
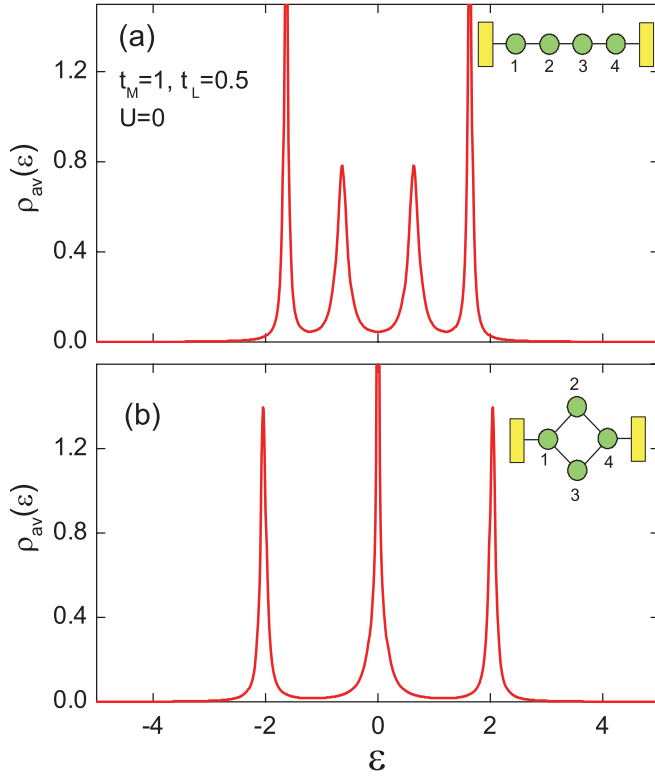
$$(17)$$

FIG. 4. (Color online) Noninteracting local DOS averaged over all sites for (a) linear and (b) ring molecules ($N = 4$) between two semi-infinite leads. The molecular configurations are depicted in the insets. $t_M = 1$, $t_L = 0.5$, and $U = 0$. Imaginary part of energy, $\gamma = 0.01$.

among which ψ_2 and ψ_3 are degenerate at $\epsilon = 0$. Since ψ_2 has no amplitude on sites 1 and 4, which are coupled to the leads, ψ_2 remains a truly localized interface state, even when the coupling to the leads is introduced, so that it makes a δ function contribution to $\rho_{av}(\epsilon)$. To avoid this singularity, an artificial imaginary energy $\gamma = 0.01$ is used in Fig. 4 for this level. The widths of the other levels correspond to the physical broadening. It should be noted that, once U is switched on, ψ_2 and ψ_3 are mixed, so that both states become delocalized.

B. Coulomb blockade

It should be emphasized that, in contrast to bulk systems, where the ratio U/t (or U/W) provides a measure of the strength of electron correlations, in the present case an important parameter characterizing the electronic structure of the interacting molecule in the vicinity of molecular level e_m is the ratio U/Γ_m, where Γ_m is the level width defined in Eq. (16). For $U/\Gamma_m \ll 1$, the molecule is expected to be in the ballistic regime where correlation effects are dominated by the molecule-lead hybridization. On the other hand, for $U/\Gamma_m \gg 1$, the molecule is in the Coulomb blockade regime where the onsite Coulomb repulsion hinders the addition of the second electron to the molecule when the first one occupies a resonant level.

Figure 5(a) shows $\bar{\rho}_{1(3)}(\mu) = -G_{11(33)}(\beta/2)$ for a chain molecule ($N = 3$) as a function of μ for three values of the contact integral t_L. The other parameters, $t_M = 1$, $U = 2$,
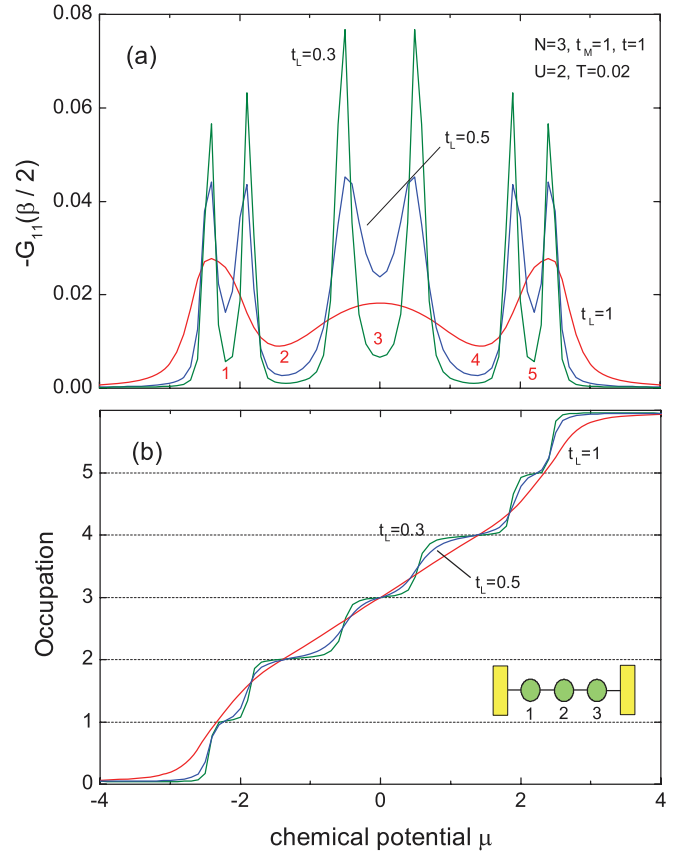

FIG. 5. (Color online) (a) Partially integrated local one-electron DOS, $\bar{\rho}_1(\mu) = -G_{11}(\beta/2)$, of a linear molecule with $N = 3$ as a function of chemical potential μ for $t_L = 0.3$, 0.5, and 1.0 ($U = 2$, $t_M = 1$, and $T = 0.02$). Small numbers near the minima of these curves indicate chemical potentials giving integer occupations. (b) Electron occupation for the same parameter set as in panel (a).

and $T = 0.02$, are common to all curves. The integrated local one-electron DOS of site 2, $\bar{\rho}_2(\mu) = -G_{22}(\beta/2)$, (not shown) is similar to $-G_{11}(\beta/2)$, except that the peak structure arising from the second energy level around $\mu = 0$ is absent. Since this molecular orbital has odd parity with respect to the center of the molecule it has no weight on site 2 irrespective of the magnitude of U. For $t_L = 1$, intramolecular correlation effects are dominated by single-particle hybridization with the leads. Thus, $\bar{\rho}_1(\mu) = -G_{11}(\beta/2)$ exhibits three broad peaks as a function of μ, which originate from the energy levels of the noninteracting molecule. With decreasing t_L [increasing U/Γ_m, see Eq. (16)], the DOS peaks start exhibiting minima at their centers. For $t_L = 0.5$ and 0.3, all three peaks split into pairs of peaks separated by a pseudogap induced by Coulomb blockade. Note that, upon decreasing t_L, the double peaks on both sides of the minima become sharper, while the energy separation between them depends only weakly on t_L.

To analyze this trend, it is useful to expand the Coulomb repulsion in Eq. (1) in terms of the orbital basis of the isolated molecule. Specifically, the density-density interaction components are given by

$$\hat{H}_d = \sum_{m,n} U_{mn} \hat{n}_{\psi_m \uparrow} \hat{n}_{\psi_n \downarrow}, \qquad (18)$$

where $\hat{n}_{\psi_{m\sigma}}$ denotes the occupation of the mth orbital with spin σ. It should be noted that Eq. (18) does not contain the Coulomb repulsion between different molecular orbitals with the same spin, since the Hubbard Hamiltonian [Eq. (1)] from which Eq. (18) is derived by changing representation from the site to molecular orbital basis set, contains only the Coulomb repulsion between the up- and down-spin electrons. The Coulomb repulsion between different molecular orbitals with the same spin can be incorporated only by extending the original Hubbard model, for example, by considering intersite Coulomb repulsion energies between electrons on neighboring sites with the same spin. These interaction terms can be treated without any difficulty with the present method. However, since the purpose of the present paper is to illustrate the ED method using a simplified model, we prefer employing the standard Hubbard model Eq. (1).

For the linear molecule with $N = 3$, one has $U_{11} = U_{33} = 3U/8$, $U_{22} = U/2$, $U_{12} = U_{23} = U/4$, and $U_{13} = 3U/8$. The effect of other nondiagonal elements not included in Eq. (18) is small if U/t is not large. In the limit of small t_L, the unrestricted Hartree-Fock (UHF) approximation may then be used to estimate the mean-field values of the mth molecular level with spin σ:

$$\tilde{e}_{m\sigma} = e_m + \sum_n U_{mn} \langle \hat{n}_{\psi_n, -\sigma} \rangle. \tag{19}$$

Thus, the first molecular level yields peaks at $-\sqrt{2}t - U/2$ and $-\sqrt{2}t - U/8$, with a gap $3U/8$. The second level has peaks at $-U/4$ and $U/4$, with a gap $U/2$, while those of the third level are located at $\sqrt{2}t + U/8$ and $\sqrt{2}t + U/2$, with a gap $3U/8$. The energy positions of the DOS peaks in Fig. 5(a) are seen to be in fair agreement with these estimates.

Figure 5(b) shows the total electron occupation of the molecule, summed over spin and site components, as a function of μ. For $t_L = 1$, the occupation varies smoothly from zero to six. In contrast, for $t_L = 0.3$ it exhibits distinct plateaus at each integer occupation, where those corresponding to odd integers are caused by the Coulomb blockade effect and their energy positions coincide with those of the pseudogaps shown in panel (a).

To illustrate the effect of Coulomb correlations in the vicinity of the pseudogap, we plot in Fig. 6 the imaginary part of the diagonal element of the self-energy, $\mathrm{Im}\Sigma_{11}(i\omega_n)$, for a chain molecule with $N = 3$. The three curves correspond to $t_L = 1$, 0.5, and 0.3. The other parameters are the same as in Fig. 5. Panel (a) shows the self-energy at half-filling ($\mu = 0$). For $t_L = 1$, the system is Fermi-liquid-like since $\mathrm{Im}\Sigma_{11}(i\omega_n)$ tends to zero linearly as $\omega_n \to 0$. This behavior is in accord with the shape of the corresponding partially integrated DOS, $\bar{\rho}_1(\mu) = -G_{11}(\beta/2)$, shown in Fig. 5(a), which exhibits a quasiparticle peak at $\mu = 0$. As discussed above, with decreasing t_L, a Coulomb pseudogap centered at $\mu = 0$ begins to be formed. As a consequence, at $t_L = 0.5$, $\mathrm{Im}\Sigma_{11}(i\omega_n)$ exhibits a finite value at small ω_n, indicating that electrons at the chemical potential have a finite lifetime inside the molecule at $T = 0.02$. Upon decreasing t_L further, $\mathrm{Im}\Sigma_{11}(i\omega_n)$ begins to approach the $1/\omega_n$ divergent behavior at small ω_n, which corresponds to the limit of an isolated molecule.
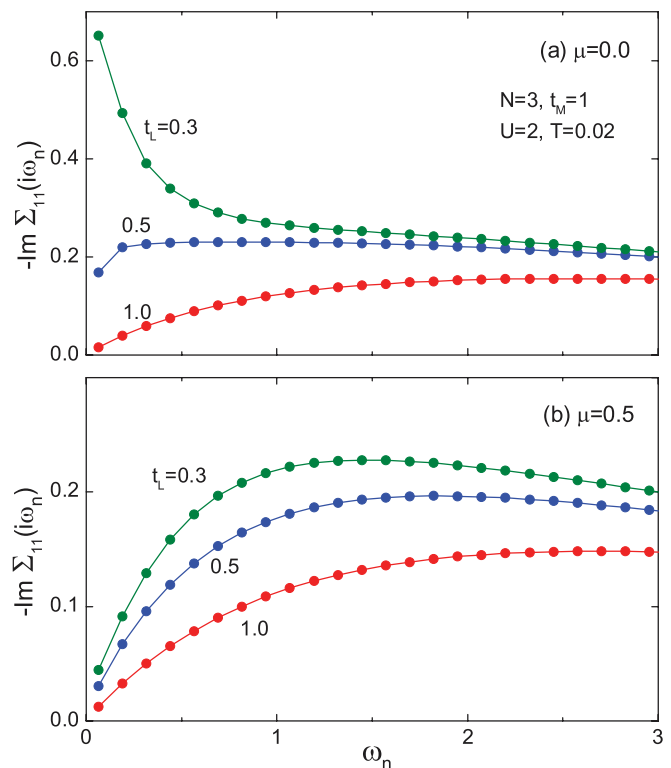

FIG. 6. (Color online) Imaginary part of correlation-induced self-energy, $-\mathrm{Im}\Sigma_{11}(i\omega_n)$, for a linear molecule with $N = 3$ at (a) $\mu = 0$ (half-filling) and (b) $\mu = 0.5$, for three values of molecule-lead coupling t_L; $U = 2$, $t_M = 1$, and $T = 0.02$.

For comparison, panel (b) illustrates the self-energy at $\mu = 0.5$, where the DOS exhibits a peak even at small values of t_L [see $-G_{11}(\beta/2)$ in Fig. 5(a) for $t_L \leqslant 0.5$]. In this case, $\mathrm{Im}\Sigma_{11}(i\omega_n)$ remains approximately linear in ω_n even at $t_L = 0.3$, indicating that, outside the pseudogap region, the molecule maintains Fermi-liquid behavior. Eventually, of course, in the limit $t_L \to 0$, the metallic behavior breaks down when the molecule no longer hybridizes with the leads.

C. Kondo effect

We now discuss the temperature dependence of the electronic structure of the $N = 3$ chain molecule. As shown in the Appendix, a cluster consisting of five levels adequately simulates a semi-infinite lead down to $T \approx 1/800$. Since the embedding potential is not affected by the size of the molecule, we use $M = 5$ lead clusters to investigate the molecular correlation effects in a wide range of temperatures. Figure 7 shows the imaginary part of the {11} element of the interacting Green's function and the self-energy as a function of Matsubara frequency for $T = 1/25, \ldots, 1/800$ and $t_L = 0.5$ at half-filling. The other parameters are the same as in Fig. 6(a). We note here that, in the limit of small ω_n, $-\pi^{-1}\mathrm{Im}G_{11}(i\omega_n)$ coincides with $\tilde{\rho}_1(\omega = 0)$, the local one-electron DOS at the chemical potential at site 1, as indicated in Eq. (14). As shown in panel (a), a sharp quasiparticle peak is formed at $\omega = 0$ when T decreases below about $1/500$. Evidently, this peak may be identified as the Kondo resonance caused by the coupling between the
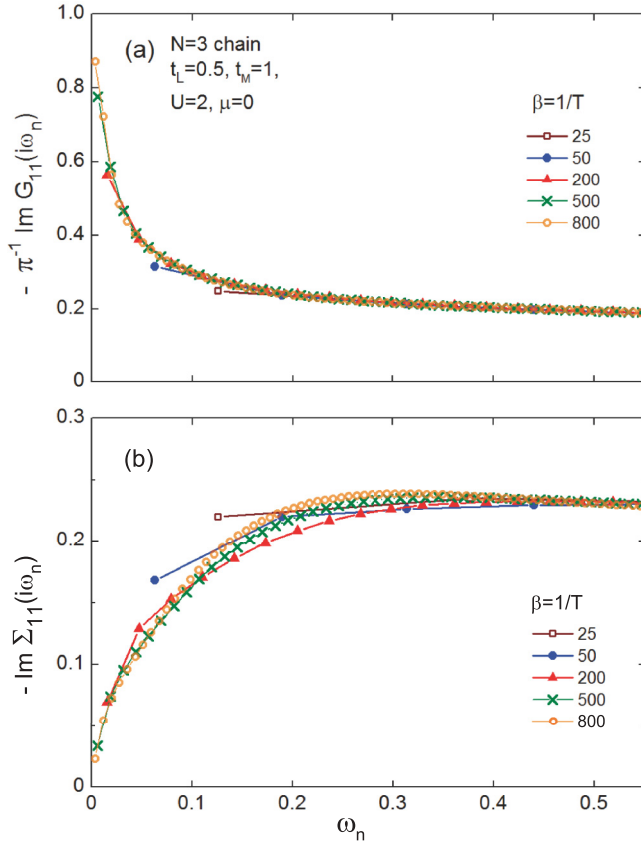
FIG. 7. (Color online) Imaginary part of (a) interacting Green's function, $\mathrm{Im}\,G_{11}(i\omega_n)$, and (b) correlation-induced self-energy, $\mathrm{Im}\,\Sigma_{11}(i\omega_n)$, for a linear molecule with $N = 3$ for four inverse temperature values, $\beta = 25, 50, 200, 500,$ and 800; $U = 2$, $t_L = 0.5$, $t_M = 1$, and $\mu = 0.0$ (half-filling).

localized spin in the half-filled second molecular level and the conduction electrons in the leads. The behavior of the self-energy is consistent with this trend, as shown in panel (b). While $-\mathrm{Im}\,\Sigma_{11}(i\omega_n)$ for $T = 0.02$ and 0.04 extrapolates to a finite value in the limit of $\omega_n \to 0$, at lower T it becomes linear in ω_n. Thus, with decreasing T the system undergoes a transition from the Coulomb blockade regime to the Kondo regime.

Since the second molecular level is energetically well separated from levels 1 and 3, its Kondo temperature may be estimated as follows. The wave function of this level in the site basis is given by

$$|\psi_2\rangle = \frac{1}{\sqrt{2}}\left(|1\rangle - |3\rangle\right)$$

and the hybridization strength defined in Eq. (16) is

$$\Gamma_2 = \pi t_L^2 [\rho_0(0) + \rho_4(0)]/2 = \pi t_L^2 \rho_0(0) = 0.131.$$

Moreover, as pointed out above, the effective Coulomb interaction for this level is $u = U_{22} = U/2 = 1$. Thus, within the context of the half-filled Anderson model, we have $u/\Delta \gg 1$, where Δ corresponds to $\Gamma_2 = 0.131$. The Kondo temperature is then approximately given by the expression[52]

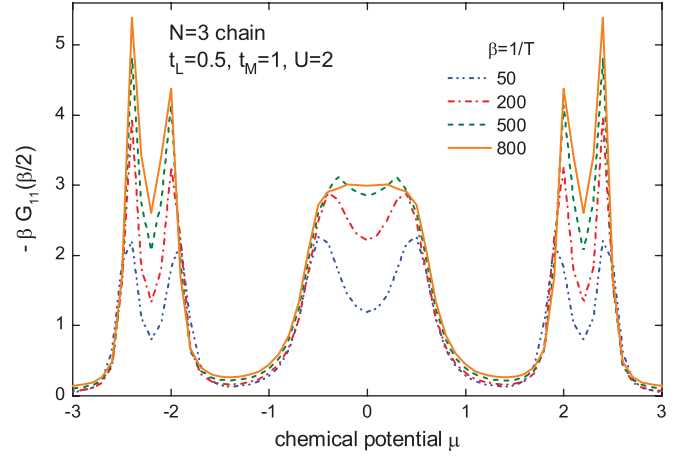$$T_K = (u\Delta/2)^{1/2} e^{-\pi u/8\Delta + \pi\Delta/2u} = 0.0157. \qquad (20)$$

FIG. 8. (Color online) Partially integrated local one-electron DOS, $\bar{\rho}_1(\mu) = -G_{11}(\beta/2)$ (multiplied by β), of a linear molecule with $N = 3$ as a function of chemical potential μ for $T = 1/50$, $1/200$, $1/500$, and $1/800$; $t_L = 0.5$, $t_M = 1$, and $U = 2$.

This estimate is fully consistent with the results in Fig. 7, where both the Green's function and correlation-induced self-energy exhibit no noticeable changes as a function of temperature for $T \lesssim T_K$. Moreover, from the initial slope of $\mathrm{Im}\,\Sigma_{11}$ we obtain a quasiparticle weight $Z \approx 1/8$, yielding[53] $T_K = \pi Z\Delta/4 \approx 0.013$, in reasonable agreement with the estimate quoted above.

Figure 8 shows the temperature dependence of the partially integrated local one-electron DOS at site 1, $\bar{\rho}_1(\mu) = -G_{11}(\beta/2)$, for the same molecule as in Fig. 7. To compare different temperatures, the curves are multiplied by β since the weight function $F(\omega)$ in Eq. (15) has integrated weight πT. As discussed above, the Kondo resonance appears at μ for $T \lesssim T_K$, where T_K depends on μ. Apparently, T_K associated with the second molecular level is larger than or comparable to the lowest value $T = 1/800$ in Fig. 8. Since the Kondo resonance appears at an energy close to $\mu = 0$, it makes a large contribution to $\bar{\rho}_1(\mu)$. As a consequence, the minimum (Coulomb pseudogap) between the two peaks for the second molecular level for $T = 0.02$ becomes shallower with decreasing T and is eventually replaced by a broad single peak at $T = 1/800$.

Interestingly, in contrast to this behavior of the second molecular level, the Coulomb pseudogaps for the first and third levels remain visible for the whole T range in Fig. 8. The difference arises from the lower T_K values for these levels. The wave function of the first level of the isolated molecule is

$$|\psi_1\rangle = \tfrac{1}{2}(|1\rangle + \sqrt{2}|2\rangle + |3\rangle),$$

and the hybridization strength is

$$\Gamma_1 = \pi t_L^2 [\rho_0(\tilde{e}_1) + \rho_4(\tilde{e}_1)]/4 = \pi t_L^2 \rho_0(\tilde{e}_1)/2 = 0.046,$$

where $\tilde{e}_1$ denotes the centroid of the doublets, $-\sqrt{2}t - 5U/16 = -2.04$. By inserting $\Delta = \Gamma_1$ and $u = U_{11} = 3U/8 = 0.75$ in Eq. (20) for the case of half-filling, we obtain $T_K = 2.4 \times 10^{-4}$, which is much lower than the temperature range in Fig. 8.
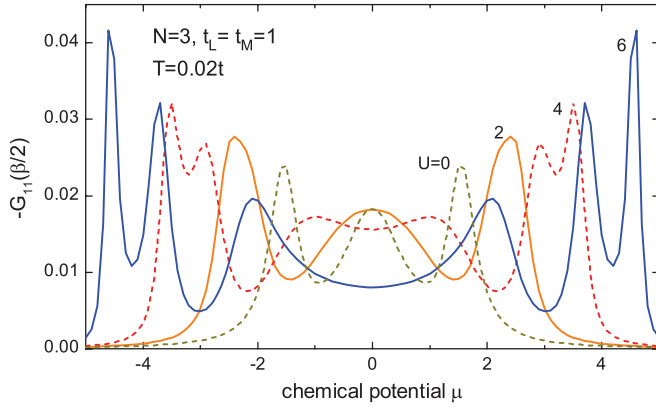
FIG. 9. (Color online) Partially integrated local one-electron DOS, $\bar{\rho}_1(\mu) = -G_{11}(\beta/2)$, of a linear molecule with $N = 3$ as a function of chemical potential μ for $U = 0$, 2, 4, and 6; $t_L = 1$, $t_M = 1$, and $T = 0.02$.

D. Large U region

In Fig. 5, we fixed the onsite Coulomb repulsion U and varied the hopping integral between leads and molecule. Alternatively, it is of interest to inquire how the molecular electronic structure changes when U is increased for fixed hopping. Here we consider the case of strong coupling where $t_L = t_R = 1$. Figure 9 shows the partially integrated local one-electron DOS at site 1, $\bar{\rho}_1(\mu) = -G_{11}(\beta/2)$, for a chain molecule with $N = 3$ as a function of μ for four values of U. The other parameters are the same as in Fig. 5. As $T/t_L \ll 1$, for $U = 0$, $-G_{11}(\beta/2)$ is nearly identical to the noninteracting local DOS at site 1, $\rho_1(\mu)$, except for a constant factor. The curve for $U = 2$ coincides with the one shown in Fig. 5(a). Compared with the bare noninteracting DOS, the three peaks are considerably broadened as a result of the intra- and intermolecular orbital Coulomb terms appearing in Eq. (18). Moreover, the outer peaks are shifted to higher energies relative to the corresponding peaks at $U = 0$. When the Coulomb energy is increased to $U = 4$, all three DOS peaks begin to exhibit a minimum at their center. Finally, they evolve into double-peak structures at $U = 6$.

Interestingly, the energy separations between the double peaks in Fig. 9 differ from those in the UHF approximation discussed above ($3U/8 = 2.25$ for the first and third orbitals and $U/2 = 3$ for the second orbital). This indicates that the off-diagonal Coulomb matrix elements ignored in Eq. (18) become progressively more important with increasing U/t. Consequently, for $U = 6$, the three orbitals are significantly mixed by these off-diagonal terms. The spectrum may then more correctly be interpreted in terms of upper and lower Hubbard bands, each consisting of three peaks and split by the Mott-like gap at the center. Nevertheless, due to the proximity effect the DOS remains finite even at low energies because the molecule is strongly coupled to the two metallic leads.

E. Chain vs ring molecules

So far we have presented results for a chain molecule with $N = 3$. The results for other linear molecules that we have studied ($N = 2$ to 5) are qualitatively similar and can be summarized as follows: (i) For a weakly correlated molecule,

the local one-electron DOS at the chemical potential μ exhibits N peaks corresponding to the N energy levels e_m of the molecule, whose width is determined by the hopping integral between the lead and molecule, t_L. (ii) With increasing U/Γ_m, these peaks start exhibiting minima at their centers. (iii) When U/Γ_m is increased further, each local one-electron DOS peak becomes a double-peak structure, so that $\bar{\rho}_i(\mu) = -G_{ii}(\beta/2)$ consists of $2N$ quasiparticle peaks as a function of μ, instead of the N peaks in the noninteracting limit. In the range of the correlation-induced pseudogaps, the electron self-energy exhibits a finite scattering rate. Furthermore, the electron occupation of the molecule as a function of μ exhibits plateaus at odd integers, whose energy positions correspond to the location of the Coulomb pseudogaps. (iv) When the temperature is lowered to reach T_K, which depends strongly on the Hamiltonian parameters and the molecular levels, Kondo resonances are formed in the Coulomb pseudogaps as a result of the strong coupling of the localized spin and conduction electrons in the leads.

As an example, we plot in Fig. 10(a) the quantity $-G_{av}(\beta/2)$, which is defined as the average of $\bar{\rho}_i(\mu) = -G_{ii}(\beta/2)$ over the N molecular sites, for a linear molecule with $N = 4$ for two values of the molecule-lead coupling parameter, $t_L = 0.3$ and 0.5. The other parameters, $U = 2$, $t_M = 1$, and $T = 0.05$, are the same as in Fig. 5. The comparison of Figs. 4 and 10 illustrates how the local one-electron DOS peaks at the chemical potential μ evolve when the onsite Coulomb energy is increased from zero to a finite value. As mentioned above, there is a one-to-one correspondence between the DOS peaks in Fig. 4 and the double-peak structures in Fig. 10. For the present molecule, the intra- and inter-molecular-orbital Coulomb energies are calculated as $U_{mm} = 3U/10$ ($m = 1$ to 4), $U_{12} = U_{13} = U_{24} = U_{34} = U/5$, and $U_{14} = U_{23} = 3U/10$. Thus, at positive μ, the DOS peaks of the third molecular orbital within the UHF approximation and in the small t_L limit are located at $(\sqrt{5} - 1)t/2$ and $(\sqrt{5} - 1)t/2 + 3U/10$, with a gap $3U/10$, while those of the fourth level appear at $(\sqrt{5} + 1)t/2 + U/5$ and $(\sqrt{5} + 1)t/2 + U/2$, also with a gap $3U/10$. The peaks at negative μ are located symmetrically with respect to $\mu = 0$. The Coulomb pseudogaps in Fig. 10(a) are in fair agreement with these mean-field values.

Finally, we discuss the ring molecule with $N = 4$ since it behaves quite differently from the corresponding linear molecule at low temperatures when it is half-filled. In Fig. 10(b) we plot $-G_{av}(\beta/2)$ of this molecule for the same parameter set as for the linear molecule in Fig. 10(a). With the molecular orbitals defined in Eq. (17), the intraorbital Coulomb energies are $U_{11} = U_{44} = U/4$, $U_{22} = U_{33} = U/2$, while the interorbital ones are $U_{mn} = U/4$ ($m \neq n$), except for $U_{23} = 0$. Hence, the DOS peaks of the first (fourth) level appear at $-2t - U/2$ and $-2t - U/4$ ($2t + U/4$ and $2t + U/2$), with a gap $U/4$, while the degenerate peaks of the second and third levels are located at $-U/4$ and $U/4$, with a twice larger gap $U/2$. The peak energies in Fig. 10(b) are in agreement with these UHF estimates. The ring molecule is half-filled when μ is located inside the pseudogap between the doublets at $\mu \sim \pm U/4$, with the first level essentially fully occupied and with the second and third ones singly occupied.
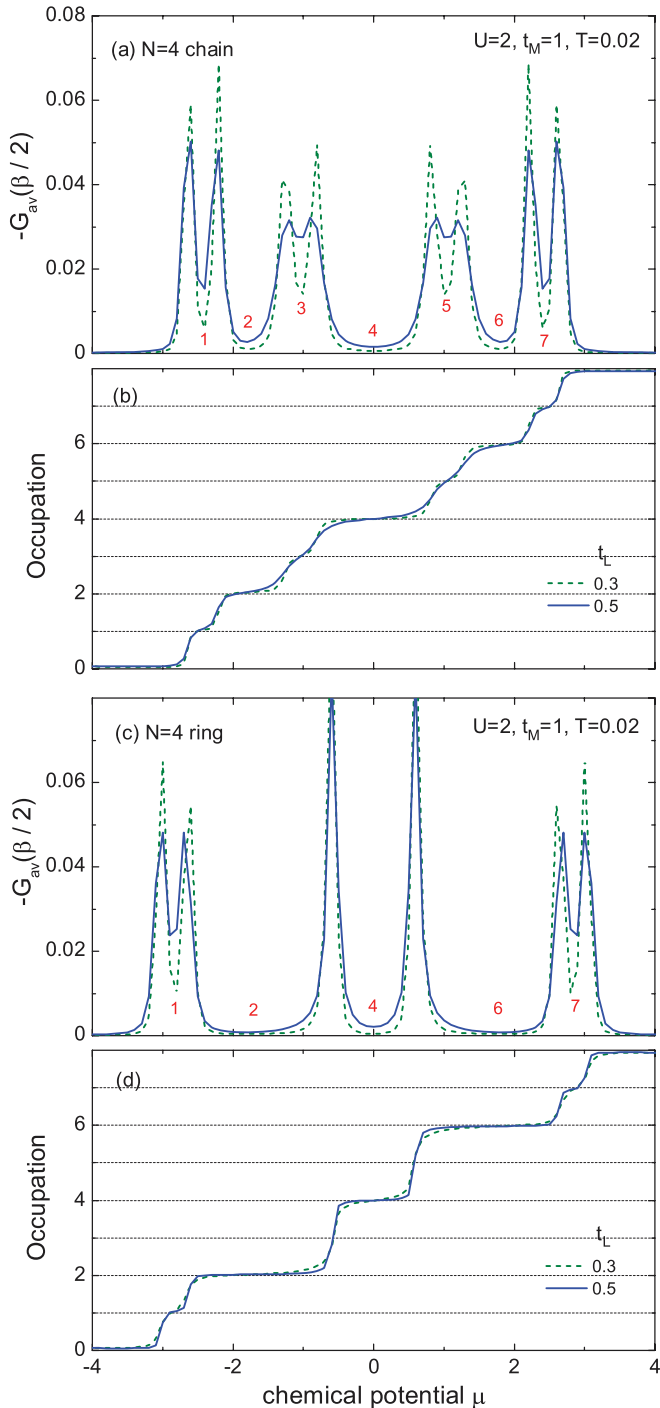
FIG. 10. (Color online) Partially integrated local one-electron DOS averaged over all the sites, $-G_{av}(\beta/2)$, for a (a) linear and (c) ring molecule with $N = 4$ for $U = 2$, $t_M = 1$, and $T = 0.02$. Solid (blue) and dashed (green) lines correspond to $t_L = 0.5$ and $t_L = 0.3$, respectively. The corresponding local densities of states for the noninteracting molecules ($U = 0$) are shown in Fig. 4. Small numbers near the minima of these curves indicate chemical potentials giving integer occupations. Panels (b) and (d) provide the corresponding occupancies as a function of μ.

The question arises as to whether the electrons in the second and third levels form a singlet or triplet state in the many-body ground state[54–56] which may arise as a consequence of
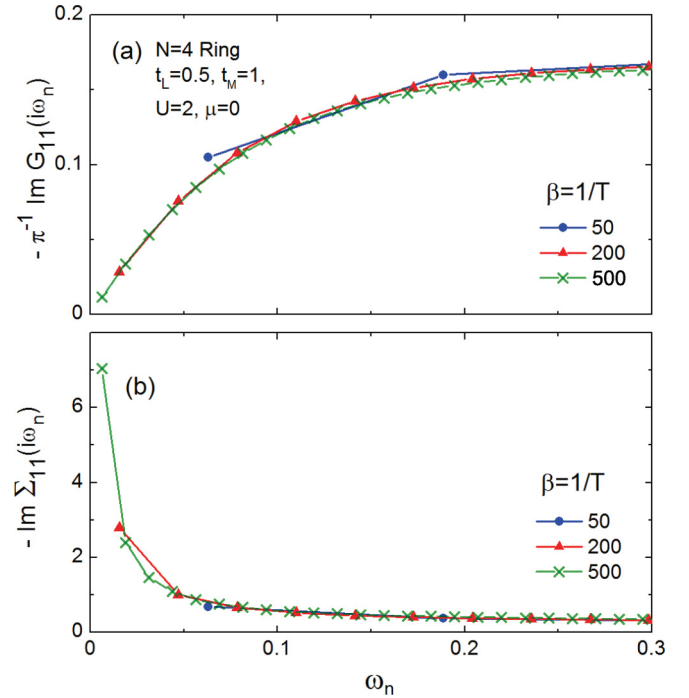

FIG. 11. (Color online) Imaginary part of (a) interacting Green's function, $\mathrm{Im}G_{11}(i\omega_n)$, and (b) correlation-induced self-energy, $\mathrm{Im}\Sigma_{11}(i\omega_n)$, for a ring molecule with $N = 4$ for inverse temperature values, $\beta = 50$, 200, and 500; $U = 2$, $t_L = 0.5$, $t_M = 1$, and $\mu = 0.0$ (half-filling).

off-diagonal Coulomb matrix elements neglected in Eq. (18). For the isolated molecule with the same U, we found that the singlet state has a lower energy. Thus, because of the absence of a localized-spin degree of freedom, the $N = 4$ ring molecule at half-filling exhibits no Kondo proximity effect. To confirm this, we plot in Fig. 11 the {11} element of the interacting Green's function and self-energy at half-filling. In striking contrast to Fig. 7 for the linear molecule with $N = 3$, the correlation-induced self-energy is seen to preserve non-Fermi-liquid behavior at low temperatures, and $\tilde{\rho}(\omega = 0)$; that is, the low-frequency limit of $-\pi^{-1}\mathrm{Im}G_{11}(i\omega_n)$ in panel (a) does not exhibit a Kondo resonance. This explains why $-G_{av}(\beta/2)$ in Fig. 10(b), when μ is located inside the pseudogap ($|\mu| \lesssim U/4$), is much smaller than the corresponding one for the linear molecule with $N = 3$ shown in Fig. 5(a), despite the fact that the pseudogap is nearly the same ($\sim U/2$) for both molecules.

IV. SUMMARY

A method for the evaluation of the electronic properties of strongly correlated molecules coupled to semi-infinite metallic leads is proposed. By simulating the surface Green's functions of the leads in terms of small clusters, the many-body interactions of the combined system in the zero bias-voltage limit are obtained via ED. The auxiliary energies and hopping terms of the lead clusters are derived by fitting the lead surface Green's functions at imaginary Matsubara frequencies. These fits are found to be sufficiently accurate to describe the Kondo physics, except in the limit of extremely low temperatures. For moderate onsite Coulomb energies within the molecule, the density of states peaks of the noninteracting

molecule are shown to split into doublets separated by correlation-induced pseudogaps. The molecular self-energy then exhibits a finite scattering rate, as expected in the regime of Coulomb blockade. Outside the pseudogap regions, the self-energy retains ordinary Fermi-liquid behavior, characteristic of ballistic transport across the molecule. The one-electron hybridization between molecule and leads is shown to be a key parameter that governs the transition between the ballistic and Coulomb blockade regimes. If the chemical potential is located inside a pseudogap, the molecular levels are integer occupied, so that a Kondo resonance appears upon lowering the temperature in the case of odd integer occupancies. The present results suggest that the approach discussed in this work for molecules or quantum dots connected to metallic leads can describe, as a function of Hamiltonian parameters, electron filling, and temperature, the full range of phenomena from Coulomb blockade to Kondo physics. While this method cannot be applied to nonequilibrium phenomena such as electron transport in the presence of a finite bias voltage, at least within the linear response regime, it is possible to study transport properties by using the equilibrium Green's function. In future applications it would be interesting to apply this scheme to the Kondo physics of molecules adsorbed on metals, multiorbital dots, and a variety of other models of interest for nanoscale devices.

APPENDIX: SINGLE ADATOM ON A SEMI-INFINITE LEAD

In Sec. II, we have discussed the main new feature of the present scheme, namely, the simulation of the semi-infinite leads in terms of a finite set of levels. Essentially, the true embedding potentials which have continuous spectra at real energies are replaced by those for finite clusters comprising a discrete set of poles. The criterion for this substitution is that along the Matsubara axis both versions of the embedding potentials should agree well for a given cluster size. Evidently, this fitting is accurate only at not-too-low temperature when the lowest Matsubara point is not too close to the real energy axis. Thus, for each cluster size, there should be a low temperature limit down to which the discrete set of levels accurately mimics the electronic properties of the actual semi-infinite lead. This limit may be determined by performing calculations for clusters with different sizes and by checking the consistency of the corresponding results.

For this purpose we consider here the special case of a single atom ($N = 1$) adsorbed on a single semi-infinite lead which is equivalent to the single-impurity Anderson model. The electronic structure of the correlated atom can therefore be directly compared with predictions within NRG.[16–22,52] If the lead is replaced by a cluster containing M levels, the

calculation of the Green's function of the combined system involves the eigenstates of a $(M + 1)$-level cluster. To be specific, we choose hopping parameters $t_M = 1$ and $t_L = 0.5$. The Coulomb interaction is assumed to have the values $U = 1$ and $U = 2$. For the simple-cubic structure of the lead, the local density of states at $\mu = 0$ in the surface layer is $\rho_s(0) = 0.52/\pi$, so that the effective hybridization between atom and lead is $\Delta = \pi t_L^2 \rho_s(0) = 0.13$. In Kondo physics, it is customary to introduce the parameter $x = U/(\pi \Delta)$ to characterize the importance of Coulomb repulsion versus single-electron hopping. Thus, for $U = 1$ and $U = 2$, this parameter has the values $x = 2.43$ and $x = 4.86$, respectively. According to Eq. (20), the Kondo temperature then has the values $T_K = 0.0157$ for $U = 1$ and $T_K = 0.001$ for $U = 2$.

As discussed in Ref. 43, finite-temperature ED can now be carried out for clusters involving up to about $n_s = 15$ levels. Here we consider lead clusters up to $M = 11$, that is, $n_s = 12$. As shown below, these sizes are sufficient for temperatures down to about $T = 1/1600$, that is, well within the Kondo regime for $U = 1$ and above about $0.6 T_K$ for $U = 2$. Increasing M to 14 would permit the study of even lower temperatures.

Also, we point out here that, while the fitting of the lead Green's function in Eq. (10) is usually done by using the Matsubara points corresponding to the physical temperature T in Sec. III, it is possible to introduce a fictitious Matsubara grid independently of T, which is used only for the purpose
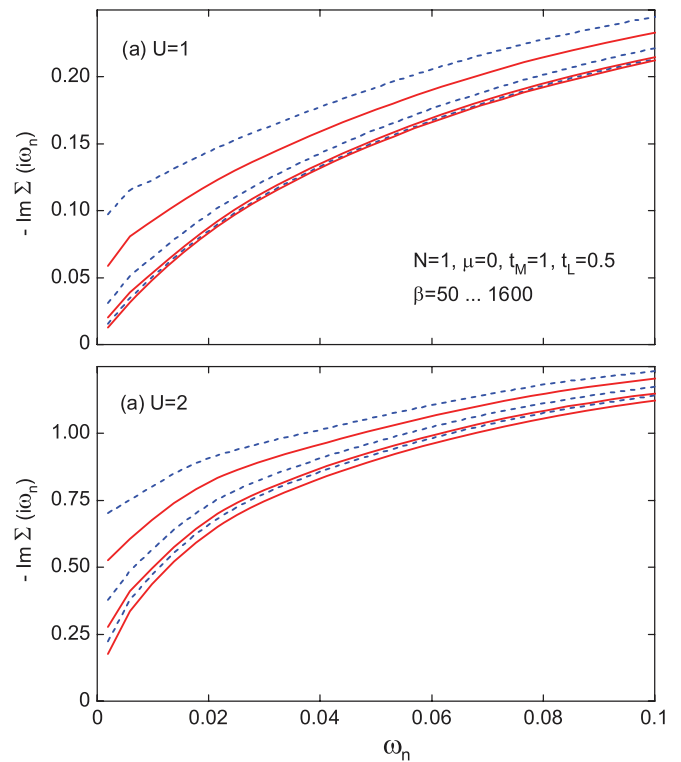

FIG. 12. (Color online) Imaginary part of self-energy of single atom on semi-infinite lead along Matsubara axis at half-filling for temperatures corresponding to $\beta = 1/T = 50, 100, 200, \ldots, 1600$ (from above). (a) $U = 1$ and (b) $U = 2$; $t_M = 1$, $t_L = 0.5$. All results are obtained for $M = 11$, with a fixed Matsubara grid corresponding to $\beta_M = 1600$.

of fitting the lead Green's function, that is, for finding the parameter set $\{\epsilon_k, v_k\}$. We denote this fictitious Matsubara temperature by T_M. Because of the large cluster size ($M = 11$), we choose $T_M = 1/1600$, which should therefore provide excellent fits of g_{00} in the entire range of physical temperatures considered, $T = 1/1600, \ldots, 1/50$. The small value of T_M implies that accurate low-energy behavior of the cluster Green's function G_{ij}^{cl} is available. We caution, however, that, in using this technique, it is important to check that the cluster Green's function agrees with that of the lead not only on the fitting points in Eq. (10), but also on the real Matsubara points corresponding to the physical temperature.

Figure 12 shows the low-energy behavior of the self-energy of the adatom for various temperatures. For $U = 1$ (top panel) and T approximately less than 0.002 ($\beta > 500$), Im $\Sigma(i\omega_n)$ is linear $\sim i\omega_n$, with a slope of about 6.4, yielding a quasiparticle weight $Z \approx 0.135$. At larger temperature, the self-energy develops a finite onset, indicating a growing correlation induced low-energy scattering rate. The finite lifetime at $\mu = 0$ then implies that the pinning condition of the interacting density of states is increasingly violated. From the initial slope of the self-energy we can estimate the Kondo temperature by using the expression[53] $T_K = \pi Z \Delta/4$. Thus, $T_K \approx 0.014$ for $U = 1$, which agrees well with the estimate $T_K = 0.0157$ derived from Eq. (20). According to the lower panel, for $U = 2$

the linear region of the self-energy is confined to much lower temperatures, with a quasiparticle weight of about $Z \lesssim 0.01$ and $T_K \lesssim 0.001$. This result is also in agreement with the estimate obtained from Eq. (20).

Figure 13 shows the quasi-particle Green's function for the correlated adatom in the same temperature range as in Fig. 12. For $U = 1$ and $T < 0.002$, Im $G(i\omega_n)$ is seen to approach the same low-energy limit as the uncorrelated Green's function, as expected from the pinning condition. With increasing T, deviations from this condition become progressively larger, in correspondence with the behavior of the self-energy shown in Fig. 12. For $U = 2$, extrapolation of Im $G(i\omega \to 0)$ to the pinning condition might be feasible only at the lowest temperature, in agreement with the estimate $T_K \approx 0.001$ given above. The behavior of $G(i\omega)$ in the very-low-T region could be explored with greater accuracy by enlarging the lead cluster beyond $M = 11$.

To illustrate the accuracy of the adatom self-energy and Green's function for smaller lead clusters, we show in Fig. 14 the results for $U = 1$ and $M = 5$. For $\beta = 1600$, a comparison with the results for $M = 11$ is also provided. Although the Green's function now is less accurate at low energies because of the reduced number of cluster levels, the self-energy still exhibits the correct qualitative trend: Below about $T \leqslant 1/400$, Im $\Sigma(i\omega_n)$ is linear in ω_n, whereas at larger T the low-energy scattering rate increases significantly. At low T, the initial slope of Im $\Sigma(i\omega_n)$ is nearly the same as for $M = 11$, yielding similar quasiparticle weight and
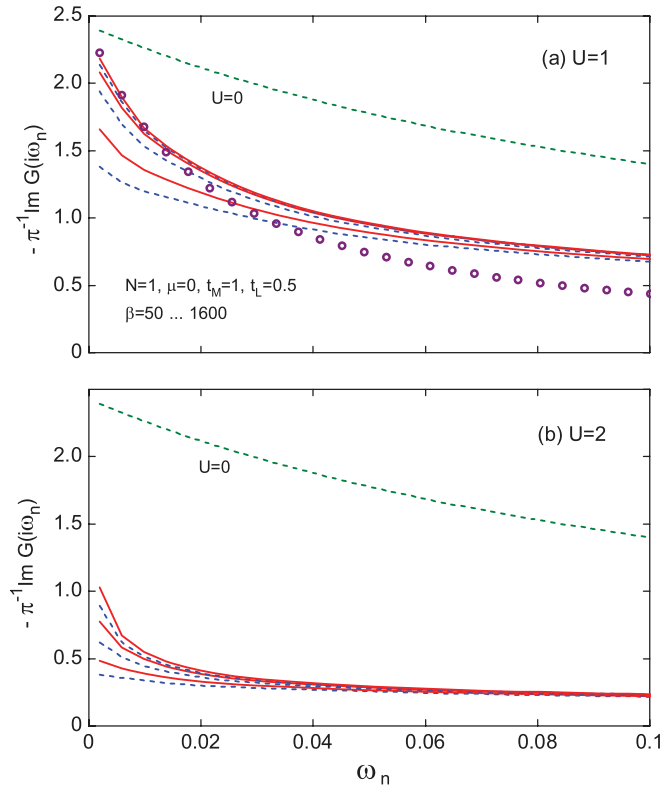

FIG. 13. (Color online) Imaginary part of Green's function of single atom on semi-infinite lead. The parameters are the same as in Fig. 12. The uncorrelated Green's function ($U = 0$) is indicated by the green dashed curve. The symbols in panel (a) correspond to the Green's function $1/(i\omega_n/Z + i\Delta)$ for a single peak at $\mu = 0$ with Kondo temperature $T_K = \pi Z \Delta/4$ (see text).
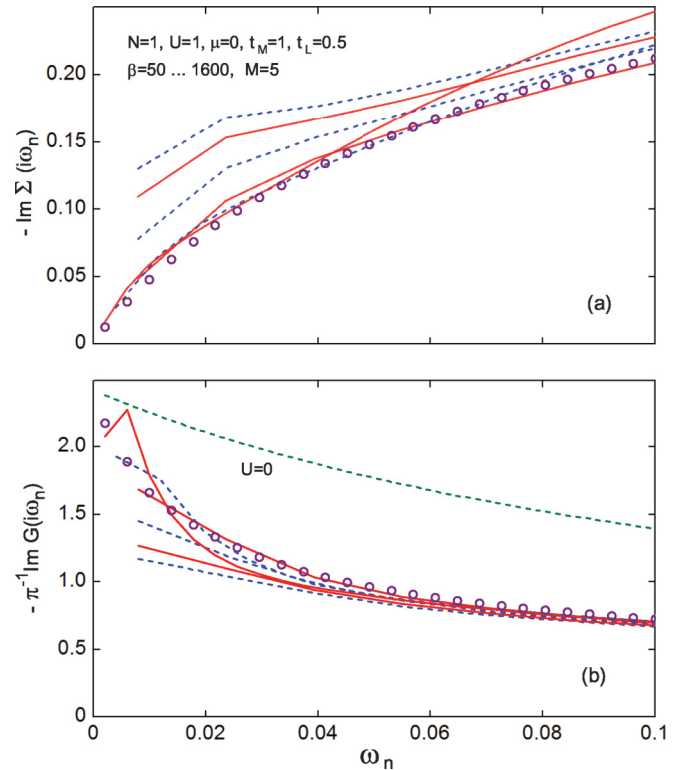

FIG. 14. (Color online) [Top (bottom)] As in top panel of Fig. 12 (13) except for $M = 5$. The Matsubara grid corresponds to $\beta_M = 1600$ for $\beta \geqslant 400$ and to $\beta_M = 400$ for $\beta < 400$. The results for $M = 11$ at $\beta = 1600$ are indicated by the circles.

Kondo temperature. Thus, in spite of the larger quantitative uncertainties in the case of the smaller lead cluster, the overall evolution, namely, from Fermi liquid behavior at low T to increasing low-energy scattering rates beyond about $T = 1/400$, is consistent with the more precise results for $M = 11$.

[1]K. S. Thygesen, M. V. Bollinger, and K. W. Jacobsen, Phys. Rev. B **67**, 115404 (2003).

[2]M. Brandbyge, J.-L. Mozos, P. Ordejón, J. Taylor, and K. Stokbro, Phys. Rev. B **65**, 165401 (2002).

[3]M. Di Ventra and N. D. Lang, Phys. Rev. B **65**, 045402 (2001).

[4]K. Hirose and M. Tsukada, Phys. Rev. B **51**, 5278 (1995).

[5]D. Wortmann, H. Ishida, and S. Blügel, Phys. Rev. B **66**, 075113 (2002).

[6]Y. Meir, N. S. Wingreen, and P. A. Lee, Phys. Rev. Lett. **66**, 3048 (1991).

[7]S. Hershfield, J. H. Davies, and J. W. Wilkins, Phys. Rev. Lett. **67**, 3720 (1991).

[8]Y. Meir, N. S. Wingreen, and P. A. Lee, Phys. Rev. Lett. **70**, 2601 (1993).

[9]P. Werner, T. Oka, M. Eckstein, and A. J. Millis, Phys. Rev. B **81**, 035108 (2010).

[10]S. Smirnov and M. Grifoni, Phys. Rev. B **84**, 125303 (2011).

[11]F. Goyer and M. Ernzerhof, J. Chem. Phys. **134**, 174101 (2011).

[12]E. V. Anda, G. Chiappe, C. A. Büsser, M. A. Davidovich, G. B. Martins, F. Heidrich-Meisner, and E. Dagotto, Phys. Rev. B **78**, 085308 (2008).

[13]Y. Asai and H. Fukuyama, Phys. Rev. B **72**, 085431 (2005).

[14]A. Oguri, J. Phys. Soc. Jpn. **70**, 2666 (2001).

[15]A. Oguri, Phys. Rev. B **63**, 115305 (2001).

[16]A. Oguri and A. C. Hewson, J. Phys. Soc. Jpn. **74**, 988 (2005).

[17]T. Numata, Y. Nisikawa, A. Oguri, and A. C. Hewson, Phys. Rev. B **80**, 155330 (2009).

[18]Y. Tanaka, N. Kawakami, and A. Oguri, Phys. Rev. B **81**, 075404 (2010).

[19]A. K. Mitchell, D. E. Logan, and H. R. Krishnamurthy, Phys. Rev. B **84**, 035119 (2011).

[20]E. Vernek, F. Qu, F. M. Souza, J. C. Egues, and E. V. Anda, Phys. Rev. B **83**, 205422 (2011).

[21]M. Misiorny, I. Weymann, and Józef Barnaś, Phys. Rev. B **86**, 035417 (2012).

[22]T. A. Costi and V. Zlatić, Phys. Rev. B **81**, 235127 (2010).

[23]D. Jacob, K. Haule, and G. Kotliar, Phys. Rev. Lett. **103**, 016803 (2009).

[24]D. Jacob and G. Kotliar, Phys. Rev. B **82**, 085423 (2010).

[25]D. Jacob, K. Haule, and G. Kotliar, Phys. Rev. B **82**, 195115 (2010).

[26]M. Karolak, D. Jacob, and A. I. Lichtenstein, Phys. Rev. Lett. **107**, 146604 (2011).

[27]B. Surer, M. Troyer, P. Werner, T. O. Wehling, A. M. Läuchli, A. Wilhelm, and A. I. Lichtenstein, Phys. Rev. B **85**, 085114 (2012).

[28]M. Romero and A. A. Aligia, Phys. Rev. B **83**, 155423 (2011).

[29]C. W. J. Beenakker, Phys. Rev. B **44**, 1646 (1991).

[30]J. König and J. Martinek, Phys. Rev. Lett. **90**, 166602 (2003).

[31]S. Braig and P. W. Brouwer, Phys. Rev. B **71**, 195324 (2005).

[32]B. Muralidharan, A. W. Ghosh, and S. Datta, Phys. Rev. B **73**, 155410 (2006).

[33]B. Song, D. A. Ryndyk, and G. Cuniberti, Phys. Rev. B **76**, 045408 (2007).

[34]D. Goldhaber-Gordon, H. Shtrikman, D. Mahalu, D. Abusch-Magder, U. Meirav, and M. A. Kastner, Nature (London) **391**, 156 (1998).

[35]S. M. Cronenwett, T. H. Oosterkamp, and L. P. Kouwenhoven, Science **281**, 650 (1998).

[36]J. Schmid, J. Weis, K. Ebert, and K. V. Klitzing, Physica B **256–258**, 182 (1998).

[37]N. Tsukahara, S. Shiraki, S. Itou, N. Ohta, N. Takagi, and M. Kawai, Phys. Rev. Lett. **106**, 187201 (2011).

[38]E. Minamitani, N. Tsukahara, D. Matsunaka, Y. Kim, N. Takagi, and M. Kawai, Phys. Rev. Lett. **109**, 086602 (2012).

[39]A. Mugarza, R. Robles, C. Krull, R. Korytár, N. Lorente, and P. Gambardella, Phys. Rev. B **85**, 155437 (2012).

[40]J. Ziroff, S. Hame, M. Kochler, A. Bendounan, A. Schöll, and F. Reinert, Phys. Rev. B **85**, 161404(R) (2012).

[41]M. Caffarel and W. Krauth, Phys. Rev. Lett. **72**, 1545 (1994).

[42]C. A. Perroni, H. Ishida, and A. Liebsch, Phys. Rev. B **75**, 045125 (2007).

[43]A. Liebsch and H. Ishida, J. Phys.: Condens. Matter **24**, 053201 (2012).

[44]A. Georges, G. Kotliar, W. Krauth, and M. J. Rozenberg, Rev. Mod. Phys. **68**, 13 (1996).

[45]G. Kotliar, S. Y. Savrasov, G. Pálsson, and G. Biroli, Phys. Rev. Lett. **87**, 186401 (2001).

[46]For recent reviews, see T. Maier, M. Jarrell, T. Pruschke, and M. H. Hettler, Rev. Mod. Phys. **77**, 1027 (2005); K. Held, Adv. Phys. **56**, 829 (2007); G. Kotliar, S. Y. Savrasov, K. Haule, V. S. Oudovenko, O. Parcollet, and C. A. Marianetti, Rev. Mod. Phys. **78**, 865 (2006).

[47]See H. Ishida and A. Liebsch, Phys. Rev. B **85**, 045112 (2012), and references herein.

[48]M. Potthoff and W. Nolting, Phys. Rev. B **59**, 2549 (1999); **60**, 7834 (1999).

[49]J. E. Inglesfield, Comput. Phys. Commun. **137**, 89 (2001).

[50]H. Ishida and A. Liebsch, Phys. Rev. B **79**, 045130 (2009).

[51]Y. Meir and N. S. Wingreen, Phys. Rev. Lett. **68**, 2512 (1992).

[52]A. C. Hewson, *The Kondo Problem to Heavy Fermions* (Cambridge University, Cambridge, 1993).

[53]A. C. Hewson, J. Phys. Soc. Jpn. **74**, 8 (2005); K. Edwards and A. C. Hewson, J. Phys.: Condens. Matter. **23**, 045601 (2011).

[54]W. Hofstetter and H. Schoeller, Phys. Rev. Lett. **88**, 016803 (2001).

[55]A. Kogan, G. Granger, M. A. Kastner, D. Goldhaber-Gordon, and H. Shtrikman, Phys. Rev. B **67**, 113309 (2003).

[56]N. Roch, S. Florens, V. Bouchiat, W. Wernsdorfer, and F. Balestro, Nature (London) **453**, 633 (2008).